Polyiron(III)−Alkoxo Clusters: A Novel Trinuclear Complex and Its Relevance to the Extended Lattices of Iron Oxides and Hydroxides

A. Caneschi,[†] A. Cornia,[‡] A. C. Fabretti,[‡] D. Gatteschi,*[,†] and W. Malavasi[‡]

Departments of Chemistry, University of Florence, Florence, Italy, and University of Modena, Modena, Italy

Received January 13, 1995[⊗]

The synthesis, solid-state structure and magnetic characterization of the complex $KFe_3(OCH_3)_7(dbm)_3{\cdot}4CH_3OH$ (**I**) (H*dbm* = dibenzoylmethane) are reported. Complex **I** readily assembles in methanolic solutions of iron(III) chloride and H*dbm* in the presence of an excess of potassium methoxide; it crystallizes in the triclinic space group $P\bar{1}$ with unit-cell parameters $a = 13.044(1)$ Å, $b = 14.174(1)$ Å, $c = 18.657(2)$ Å, $\alpha = 97.94(1)°$, $\beta = 104.13(1)°$, $\gamma = 114.12(1)°$, $V = 2940.6(6)$ Å^3, and $Z = 2$ at 190 K. Refinement of 10076 reflections with 705 parameters yielded $R = 0.046$ and $R_w = 0.051$. The solid-state molecular structure of **I** consists of a triangular array of iron(III) ions connected by a triply bridging methoxide and three μ_2-methoxide ligands. The oxygen donors of a monodentate methoxide and of a chelating *dbm* ligand complete the coordination sphere of each metal ion. The resulting mononegative $Fe_3(\mu_3\text{-}OCH_3)(\mu_2\text{-}OCH_3)_3(OCH_3)_3(dbm)_3$ moiety coordinates the K counterion through the oxygens of the μ_2-OCH_3 ligands. The oxygen atoms in the core of **I** are arranged in two essentially parallel layers and display a *closest-packing* which is found in iron oxides and hydroxides. The high-spin iron(III) ions are antiferromagnetically coupled with an $S = {}^1/_2$ spin ground state. Assumption of a C_{2v} point-group symmetry for the cluster leads to a satisfactory reproduction of the observed magnetic behavior with $g = 2.0$ and either $J = 10.6(1)$, $J' = 15.3(2)$ cm^{-1} or $J = 12.9(2)$, $J' = 9.7(1)$ cm^{-1}, where the spin-only Heisenberg Hamiltonian is defined as $\mathbf{H} = \sum_{i>j} J_{ij}\mathbf{S}_i\mathbf{S}_j$ and J' is the unique coupling constant. The relative contributions of geometrical distortions and of antisymmetric exchange to the splitting of the 4-fold ^2E electronic ground state of an idealized system with trigonal symmetry have been estimated from X-band EPR spectra recorded on powdered samples.

Introduction

In recent years, the hydrolytic chemistry of iron(III) has been actively investigated.[1−4] Polyiron(III) aggregates which exhibit some structural features typical of the extended lattices of iron(III) oxides and hydroxides have been isolated from aqueous environments containing simple iron(III) salts, a base, and suitably designed ligands which block the growth of the bulk oxides, limiting the size of the particles.[3,4] Some similarities are apparent between the structure of α-FeO(OH) (göthite)[5] and the arrangement of the oxygen atoms from OH^- and O^{2-} ligands observed in the complexes $[Fe_{17}(O)_4(OH)_{16}(heidi)_8(H_2O)_{12}]^{3+}$ (**1**) and $[Fe_{19}(O)_6(OH)_{14}(heidi)_{10}(H_2O)_{12}]^{+}$ (**2**).[4,6] Controlled hydrolysis of iron salts represents indeed an excellent route to nanostructured materials and provides a means to study the boundary between molecular and extended systems.[7−10] Interestingly, it has been shown that hydrolytic-aggregation processes can be of use in the deposition of thin-layers of iron oxides from simple iron(III) precursors by the sol−gel technique.[11]

The discovery that the catalytic sites of a number of *non-heme* iron proteins contain *oxo*- or *hydroxo*-bridged diiron units[2] and the relevance of large polyiron(II,III)-oxo aggregates to the *ferritin* core[8,10] has further encouraged this kind of studies.

Iron(II,III) polynuclear aggregates have been assembled in non-aqueous environments, taking advantage of the presence of water traces or of dioxygen to build up iron−oxo cores. Among the most recent examples are the dodecanuclear mixed-valent clusters $Fe_{12}(O)_2(CH_3CO_2)_6(CH_3O)_{18}(CH_3OH)_{4.67}$ (**3**)[9] and $Fe_{12}(O)_2(CClH_2CO_2)_{5.3}Cl_{0.7}(CH_3O)_{18}(CH_3OH)_4$ (**4**);[10] their unusual molecular architecture is based on a closely packed array

* To whom correspondence should be addressed.
[†] University of Florence.
[‡] University of Modena.
[⊗] Abstract published in *Advance ACS Abstracts,* August 1, 1995.

(1) Schneider, W. *Comments Inorg. Chem.* **1984**, *3*, 205. Schneider, W. *Chimia* **1988**, *42*, 9. Hagen, K. S. *Angew. Chem., Int. Ed. Engl.* **1992**, *31*, 1010.
(2) Lippard, S. J. *Angew. Chem., Int. Ed. Engl.* **1988**, *27*, 344 and references therein. Lippard, S. J. *Chem. Br.* **1986**, *22*, 222.
(3) Wieghardt, K.; Pohl, K.; Jibril, I.; Huttner, G. *Angew. Chem., Int. Ed. Engl.* **1984**, *23*, 77. Jameson, D. L.; Xie, C. L.; Hendrickson, D. N.; Potenza, J. A.; Schugar, H. J. *J. Am. Chem. Soc.* **1987**, *109*, 740. Harding, C. J.; Henderson, R. K.; Powell, A. K. *Angew. Chem., Int. Ed. Engl.* **1993**, *32*, 570.
(4) Powell, A. K.; Heath, S. L.; Gatteschi, D.; Pardi, L.; Sessoli, R.; Spina, G.; Del Giallo, F.; Pieralli, F. *J. Am. Chem. Soc.* **1995**, *117*, 2491.
(5) Hyde, B. G.; Andersson, S. *Inorganic Crystal Structures*; John Wiley & Sons: New York, 1989; p 72.
(6) Abbreviations used in the text: H$_3$*heidi* = $N(CH_2COOH)_2(CH_2CH_2OH)$; H*dbm* = dibenzoylmethane (1,3-diphenyl-1,3-propanedione); H*dpm* = dipivaloylmethane (2,2,4,4-tetramethyl-3,5-heptanedione); H*acac* = acetylacetone (2,4-pentanedione); *tren* = 2,2′,2″-triaminotriethylamine; H*dbsq* = 3,5-di-*tert*-butylsemiquinone; H*dbcat* = 3,5-di-*tert*-butylcatechol.
(7) Gatteschi, D. *Adv. Mater.* **1994**, *6*, 635. Gatteschi, D.; Pardi, L. *Mol. Cryst. Liq. Cryst.* **1993**, *233*, 217. Papaefthymiou, G. C. *Phys. Rev. B* **1992**, *46*, 10366. Delfs, C. D.; Gatteschi, D.; Pardi, L.; Sessoli, R.; Wieghardt, K.; Hanke, D. *Inorg. Chem.* **1993**, *32*, 3099.
(8) Micklitz, W.; McKee, V.; Rardin, R. L.; Pence, L. E.; Papaefthymiou, G. C.; Bott, S. G.; Lippard, S. J. *J. Am. Chem. Soc.* **1994**, *116*, 8061. Micklitz, W.; Lippard, S. J. *J. Am. Chem. Soc.* **1989**, *111*, 6856. Gorun, S. M.; Papaefthymiou, G. C.; Frankel, R. B.; Lippard, S. J. *J. Am. Chem. Soc.* **1987**, *109*, 3337. Gorun, S. M.; Lippard, S. J. *Nature* **1986**, *319*, 666.
(9) Taft, K. L.; Papaefthymiou, G. C.; Lippard, S. J. *Inorg. Chem.* **1994**, *33*, 1510. Taft, K. L.; Papaefthymiou, G. C.; Lippard, S. J. *Science* **1993**, *259*, 1302.
(10) Caneschi, A.; Cornia, A.; Lippard, S. J.; Sessoli, R. Unpublished results.
(11) Brinkler, C. J.; Scherer, G. W. *Sol-Gel Science: The Physics and Chemistry of Sol-Gel Processing*; Academic Press: New York, 1990. Guglielmi, M.; Principi, G. *J. Non-Cryst. Sol.* **1982**, *48*, 161.

0020-1669/95/1334-4660$09.00/0

Table 1. Crystal Data and Experimental Parameters for $KFe_3(OCH_3)_7(dbm)_3 \cdot 4CH_3OH$

chem. formula: $Fe_3KC_{56}H_{70}O_{17}$	fw = 1221.8
a = 13.044(1) Å	space group:[a] $P\bar{1}$ (No. 2)
b = 14.174(1) Å	T = 190 K
c = 18.657(2) Å	λ = 0.71069 Å
α = 97.94(1)°	ϱ_{calcd} = 1.38 g cm^{-3}
β = 104.13(1)°	μ = 8.1 cm^{-1}
γ = 114.12(1)°	R^b = 0.046
V = 2940.6(6) Å^3	$R_w{}^b$ = 0.051
Z = 2	

[a] Hahn, T., Ed. *International Tables for X-ray Crystallography*, D. Reidel: Dordrecht, The Netherlands, 1983. [b] $R = \sum||F_o| - |F_c||/\sum|F_o|$ and $R_w = \sum w^{1/2}||F_o| - |F_c||/\sum w^{1/2}|F_o|$ where $w = 2.19/[\sigma^2(|F_o|) + 3 \times 10^{-4}|F_o|^2]$.

of oxygen atoms which simulates a fragment of a face-centered cubic lattice whose octahedral interstices are occupied by iron atoms. Two μ_6-oxo ligands represent fundamental structural elements in these peculiar systems.

Our current efforts in this area involve basic alcoholic media and β-diketonates as limiting (and solubilizing) agents. β-Diketonates have complexing properties not dissimilar from those of certain biogenic ligands such as sugars, which display good limiting properties in aqueous solutions. The resulting iron(III)−alkoxo cores are excellent structural models for the corresponding oxo−hydroxo systems.

We herein report the synthesis, solid-state structure and magnetic behavior of a novel triiron(III) cluster with a "*voided-cubane*" structure which readily assembles in strongly alkaline methanolic solutions of iron(III) chloride and the ligand H*dbm*.[6]

Experimental Section

Synthesis. All operations were performed with strict exclusion of moisture, unless otherwise stated. Methanol was distilled over $Mg(OCH_3)_2$ shortly before use. H*dbm* (Aldrich, 98%) and resublimed $FeCl_3$ (Carlo Erba, 99%) were used without purification. Potassium methoxide was used as a 25% solution in methanol (Fluka).

To 10 mmol of iron(III) trichloride dissolved in 30 mL of anhydrous methanol was added a solution containing 10 mmol of H*dbm* and 40 mmol of potassium methylate in 120 mL of anhydrous methanol dropwise with stirring at 298 K. After the addition was completed, the mixture was stirred for 1 h; the yellow precipitate was then filtered off, and the resulting bright-yellow solution was allowed to stand at room temperature. Yellow rod-like crystals formed overnight; upon further standing, they were gradually replaced by yellow diamond-shaped crystals which were collected by filtration, rapidly washed with methanol, and dried under vacuum (approximate yield 70%). Both types of crystals gave satisfactory analyses for $Fe_3KC_{56}H_{70}O_{17}$. IR spectral data (KBr pellets, cm^{-1}): 3422 (br), 3061 (s), 2920 (s), 2816 (s), 1594 (s), 1549 (s), 1522 (s), 1479 (s), 1452 (s), 1376 (s), 1318 (s), 1226 (m), 1182 (w), 1072 (s), 1024 (s), 941 (w), 785 (m), 753 (m), 721 (s), 688 (s), 620 (s), 497 (s), 461 (s).

UV reflectance spectral data (nm): 375 (s), 450 (sh).

X-ray Data Collection. A yellow, diamond-shaped crystal (0.3 × 0.5 × 0.4 mm) was removed from the mother liquid, mounted on the top of a thiny glass fiber with silicon grease under a cold dinitrogen stream, and rapidly transferred to an Enraf-Nonius CAD4 diffractometer equipped with low-temperature facility and Mo-Kα graphite-monochromated radiation. Unit cell parameters were determined by least-squares fitting to the setting angles of 24 intense low-angle reflections ($9.7 < \theta < 15.0°$). The crystal quality was judged satisfactory on the basis of the average half-height width of sample reflections $\langle w_{1/2} \rangle$ = 0.29°. Crystal data and relevant experimental parameters are reported in Table 1. Laue group $\bar{1}$ was confirmed by running the program *TRACER II*.[12] All data were corrected for Lorentz and polarization effects. No absorption correction was applied to collected intensities.

Structure Solution and Refinement. The structure was solved by direct methods with the program *SIR92*,[13] which gave the positions of all non-hydrogen atoms. Refinement was carried out by using the *SHELX76* program package.[14] [10076 reflections with $F_o^2 > 4\sigma(F_o^2)$]. Anisotropic thermal parameters were refined for all non-hydrogen atoms. Hydrogen atoms H(O14) and H(O15) were located in ΔF maps, whereas all the remaining hydrogen atoms were treated as fixed contributors in calculated positions and allowed to ride on the attached carbon atoms. The hydrogen atom attached to O(16) was not located. Isotropic thermal parameters $B(H) = 1.2\ B_{eq}(X)$, where X is the parent oxygen or carbon atom, were used for all hydrogen atoms.

Final atom positional parameters for non-hydrogen atoms are reported in Table 2. Relevant bond distances and angles are summarized in Table 3. Selected non-bonded distances and angles for the KFe_3 tetrahedron can be found in Table 4.

Instrumentation and Physical Measurements. The magnetic susceptibility of a 20.2 mg microcrystalline sample was measured by using a Métronique MS03 SQUID Magnetometer in the temperature range 2.2−270 K in an applied field of 1 T. The contribution of the sample holder was determined separately in the same temperature range and field. Diamagnetic corrections were estimated from Pascal's constants.

EPR spectra of powdered samples were recorded on a Varian E9 spectrometer operating at X-band frequency, equipped with an Oxford Instruments ESR9 liquid-helium continuous-flow cryostat, in the temperature range 4.2−298 K.

Least-Squares Calculations. All calculations were performed on a CONVEX 220 computer using the E04FCF-NAG Fortran Library minimization routine.

Results and Discussion

Synthesis. The possible successful use of β-diketonates as limiting agents for the study of solvolytical aggregation processes involving iron(II,III) has been suggested by the previous isolation of low-nuclearity polyiron species containing alkoxide bridges and chelating β-diketonate ligands. Twenty years ago Gray and co-workers reported[15] the synthesis, spectroscopic and magnetic characterization of dialkoxo-bridged iron(III) dimeric complexes formulated as $Fe_2(OR)_2(L)_4$, where HL = H*acac* or H*dpm*[6] and R = CH_3, C_2H_5, or i-C_3H_7. These complexes were found to assemble readily under aerobic conditions by reaction of simple iron(II,III) salts with the ligand HL and a base using the appropriate alcohol as a solvent. More recently the tetranuclear cubane complexes $[Fe^{II}(OCH_3)(CH_3OH)(dbm)]_4$ (**5**) and $[Fe^{II}(OCH_3)(CH_3OH)(dpm)]_4$ (**6**) were isolated by Lippard *et al.*[16] as products of the reaction of iron(II) chloride with 1 equiv of β-diketone and 2 equiv of lithium methoxide in methanol under strictly anaerobic conditions.

In the course of a systematic study on the limiting properties of β-diketonates in alcoholic media, we observed that reaction of iron(III) chloride with 1 equiv of H*dbm* and 4 equiv of potassium methoxide in anhydrous methanol leads to the precipitation of a mixture of a bright yellow solid and potassium chloride. By slow evaporation of the filtered yellow solution, yellow needles[17] are obtained overnight in low yield. Upon further concentration, large diamond-shaped yellow crystals

(12) Lawton, S. L. *Tracer II: A Fortran Lattice Transformation-Cell Reduction Program*; Mobil Oil Corp.: Paulsboro, NJ, 1967.

(13) Altomare, A.; Cascarano, G.; Giacovazzo, C.; Guagliardi, A. *J. Appl. Crystallogr.* **1994**, *27*, 1045.

(14) Sheldrick, G. M. *SHELX76. Program for Crystal Structure Determination*; University of Cambridge: Cambridge, England, 1976.

(15) Wu, C.-H. S.; Rossman, G. R.; Gray, H. B.; Hammond, G. S.; Schugar, H. J. *Inorg. Chem.* **1972**, *11*, 990.

(16) Taft, K. L.; Caneschi, A.; Pence, L. E.; Delfs, C. D.; Papaefthymiou, G. C.; Lippard S. J. *J. Am .Chem. Soc.* **1993**, *115*, 11753.

Table 2. Final Atom Positional Parameters and B(eq) Values (Å^2) for $KFe_3(OCH_3)_7(dbm)_3{\cdot}4CH_3OH$[a]

atom	x/a	y/b	z/c	B(eq)[b]	atom	x/a	y/b	z/c	B(eq)[b]
Fe(1)	−0.13992(3)	0.01051(3)	0.72407(2)	1.74(1)	C(20)	0.1960(3)	0.2947(2)	0.8488(2)	2.5(1)
Fe(2)	−0.28384(3)	−0.23942(3)	0.72007(2)	1.70(1)	C(21)	0.2692(3)	0.2781(3)	0.8111(2)	3.1(1)
Fe(3)	−0.06190(3)	−0.16287(3)	0.65542(2)	1.76(2)	C(22)	0.3819(3)	0.3597(3)	0.8235(2)	3.9(1)
K	−0.34962(6)	−0.17263(6)	0.53101(4)	3.02(3)	C(23)	0.4227(3)	0.4599(3)	0.8727(2)	4.3(2)
O(1)	−0.1044(2)	−0.1165(1)	0.7546(1)	1.75(7)	C(24)	0.3493(3)	0.4769(3)	0.9095(2)	4.1(1)
O(2)	−0.3044(2)	−0.1164(1)	0.6906(1)	1.81(7)	C(25)	0.2376(3)	0.3962(2)	0.8980(2)	3.2(1)
O(3)	−0.2336(2)	−0.2673(1)	0.6293(1)	1.85(7)	C(26)	−0.1371(3)	0.1330(2)	0.9503(2)	2.4(1)
O(4)	−0.0995(2)	−0.0429(1)	0.6360(1)	1.93(7)	C(27)	−0.0923(3)	0.2253(3)	1.0092(2)	3.1(1)
O(5)	0.0302(2)	0.1305(2)	0.7738(1)	2.31(7)	C(28)	−0.1378(3)	0.2220(3)	1.0693(2)	3.8(2)
O(6)	−0.1582(2)	0.0501(2)	0.8261(1)	2.42(8)	C(29)	−0.2229(4)	0.1295(3)	1.0723(2)	4.2(2)
O(7)	−0.3176(2)	−0.2035(2)	0.8183(1)	2.20(8)	C(30)	−0.2713(5)	0.0382(3)	1.0128(3)	6.2(2)
O(8)	−0.2265(2)	−0.3342(2)	0.7710(1)	2.07(7)	C(31)	−0.2289(4)	0.0404(3)	0.9517(2)	5.0(2)
O(9)	−0.0171(2)	−0.2755(2)	0.6895(1)	2.27(8)	C(32)	−0.3966(3)	−0.2344(2)	0.9186(2)	2.2(1)
O(10)	0.1134(2)	−0.0604(2)	0.7069(1)	2.25(8)	C(33)	−0.3785(3)	−0.2409(3)	0.9933(2)	3.3(1)
O(11)	−0.1956(2)	0.0973(2)	0.6764(1)	2.65(8)	C(34)	−0.4505(4)	−0.2268(3)	1.0330(2)	3.8(2)
O(12)	−0.4446(2)	−0.3448(2)	0.6697(1)	2.61(8)	C(35)	−0.5434(4)	−0.2106(4)	0.9979(2)	4.8(2)
O(13)	−0.0535(2)	−0.1975(2)	0.5569(1)	2.55(8)	C(36)	−0.5648(4)	−0.2075(5)	0.9225(3)	7.0(3)
O(14)	−0.2228(2)	−0.1991(2)	0.4446(1)	3.5(1)	C(37)	−0.4895(3)	−0.2172(4)	0.8837(2)	5.0(2)
O(15)	−0.3345(3)	0.0166(2)	0.5313(2)	5.9(1)	C(38)	−0.1894(3)	−0.4413(2)	0.8491(2)	2.2(1)
O(16)	−0.5499(3)	−0.3314(3)	0.4181(2)	6.6(1)	C(39)	−0.2197(3)	−0.5011(2)	0.9010(2)	3.0(1)
C(1)	−0.0239(3)	−0.0952(2)	0.8298(2)	2.3(1)	C(40)	−0.1743(3)	−0.5727(3)	0.9152(2)	3.6(1)
C(2)	−0.4018(3)	−0.0975(2)	0.6979(2)	2.6(1)	C(41)	−0.1004(3)	−0.5857(3)	0.8777(2)	3.5(1)
C(3)	−0.2840(3)	−0.3714(2)	0.5785(2)	2.8(1)	C(42)	−0.0716(3)	−0.5290(3)	0.8255(2)	3.4(1)
C(4)	−0.0380(3)	0.0301(2)	0.5971(2)	2.6(1)	C(43)	−0.1164(3)	−0.4572(2)	0.8107(2)	2.7(1)
C(5)	0.0766(3)	0.2046(2)	0.8363(2)	2.3(1)	C(44)	0.0820(3)	−0.3826(2)	0.6955(2)	2.3(1)
C(6)	0.0235(3)	0.2058(2)	0.8929(2)	2.5(1)	C(45)	−0.0177(3)	−0.4714(3)	0.6439(2)	3.0(1)
C(7)	−0.0898(3)	0.1283(2)	0.8855(2)	2.3(1)	C(46)	−0.0227(3)	−0.5726(3)	0.6330(2)	3.8(1)
C(8)	−0.3238(2)	−0.2508(2)	0.8716(2)	1.9(1)	C(47)	0.0721(3)	−0.5849(3)	0.6749(2)	3.9(2)
C(9)	−0.2757(3)	−0.3209(2)	0.8850(2)	2.2(1)	C(48)	0.1708(3)	−0.4982(3)	0.7263(2)	3.6(2)
C(10)	−0.2317(2)	−0.3604(2)	0.8332(2)	2.0(1)	C(49)	0.1766(3)	−0.3968(3)	0.7371(2)	3.0(1)
C(11)	0.0839(3)	−0.2747(2)	0.7041(2)	2.2(1)	C(50)	0.3211(3)	0.0093(2)	0.7374(2)	2.5(1)
C(12)	0.1927(3)	−0.1828(2)	0.7232(2)	2.3(1)	C(51)	0.4234(3)	0.0207(3)	0.7905(2)	2.9(1)
C(13)	0.2014(3)	−0.0815(2)	0.7224(2)	2.1(1)	C(52)	0.5332(3)	0.1051(3)	0.8021(2)	3.4(1)
C(14)	−0.1827(4)	0.1966(3)	0.7140(2)	4.2(2)	C(53)	0.5421(3)	0.1785(3)	0.7591(2)	3.9(1)
C(15)	−0.5095(3)	−0.4291(3)	0.6967(3)	4.7(2)	C(54)	0.4413(3)	0.1681(3)	0.7050(2)	4.2(2)
C(16)	0.0310(4)	−0.2177(4)	0.5332(2)	4.1(2)	C(55)	0.3301(3)	0.0843(3)	0.6942(2)	3.3(1)
C(17)	−0.2571(4)	−0.2901(3)	0.3868(2)	4.5(2)	Os	−0.5930(3)	−0.3454(3)	0.5477(2)	6.8(2)
C(18)	−0.3512(4)	0.0896(4)	0.4929(3)	5.6(2)	Cs	−0.6993(4)	−0.3595(5)	0.5623(3)	7.2(3)
C(19)	−0.6456(4)	−0.3819(4)	0.3489(3)	5.6(2)					

[a] Numbers in parentheses are errors in the last significant digit. [b] $B(\text{eq}) = (8\pi^2/3)[U_{11}(aa^*)^2 + U_{22}(bb^*)^2 + U_{33}(cc^*)^2 + 2U_{12}aa^*bb^*\cos\gamma + 2U_{13}aa^*cc^*\cos\beta + 2U_{23}bb^*cc^*\cos\alpha]$.

grow in 1−2 days and gradually replace the needle-like crystals. The two crystalline phases gave very similar elemental analyses and were indeed shown by single-crystal X-ray techniques to be different crystalline forms of the novel triiron(III) cluster $KFe_3(OCH_3)_7(dbm)_3{\cdot}4CH_3OH$ (**7**). Surprisingly, use of lithium or sodium methoxide instead of potassium methoxide did not lead to the expected lithium- or sodium-containing compounds, respectively. On the basis of the available solid-state structure, we suggest that the potassium ion may exhert a specific template effect in the synthesis of **7** by virtue of its large ionic radius which allows a particularly favorable accomodation on the hollow side of the cluster.

Modifications of the above decribed synthetic procedure allowed the isolation of a surprising variety of methoxo-bridged polynuclears. In addition to the well-known dimeric species $Fe_2(OCH_3)_2(dbm)_4$ (**8**) a hexanuclear[18] and a decanuclear[19] complex were synthesized and structurally characterized. The simple coordination requirements of β-diketonates, which have been found to act almost invariably as chelating ligands, may play an important role since they turn out to be compatible with a large number of structural types. Furthermore, the molecular structure and coordination geometry of β-diketonates [RC(O)CHC(O)R] are such that the peripheral hydrophobic shell of the cluster originates mainly from the R substituents. The nature of the R groups (polarity, steric hindrance, etc.) is thus expected to have a great influence on the displayed limiting properties. *dbm* (R = C_6H_5) apparently represents a particularly favorable choice in conjunction with polar solvents such as methanol or methanol/chloroform mixtures.

Crystal Structure. Figure 1 shows an ORTEP view of compound **7**, as resulting from single-crystal X-ray measurements at 190 K. The carbon atoms of the phenyl rings of the *dbm* ligands and all hydrogen atoms except for HO(14), HO(15), and HOs have been omitted for clarity. An alternative view of the cluster along its virtual C_3 axis is presented in Figure 2. The iron atoms lie at the vertices of an equilateral triangle, the iron−iron separations being equal within experimental error (see Table 4), and display distorted octahedral coordination geometries with oxygen donors only. Peculiar to complex **7** is the triply bridging methoxide ligand O(1)−C(1), which represents a fundamental structural element. Each side of the triangle is further bridged by a μ_2-OCH_3 ligand. A chelating *dbm* and a monodentate OCH_3 ligand per iron atom complete the metal coordination environments. The organic moieties stretch out of the cluster, acting as blocks to its further growth. The

(17) $Fe_3KC_{56}H_{70}O_{17}$, fw = 1221.8; triclinic, $P\bar{1}$ (No. 2): a = 12.760(4), b = 20.854(4), c = 24.452(4) Å; α = 112.56(1), β = 100.30(2), γ = 92.42(2)°; V = 5868(2) Å^3, Z = 4; d_{calcd} = 1.38 g cm^{-3}; 14501 reflections collected at T = 220 K with Mo Kα radiation; for 8164 reflections with $F_o > 4\sigma(F_o)$ and 695 parameters, R = 0.068, R_w = 0.071.

(18) Caneschi, A.; Cornia, A.; Lippard, S. J. *Angew. Chem., Int. Ed. Engl.* **1995**, *34*, 467.

(19) Caneschi, A.; Cornia, A.; Fabretti, A. C.; Gatteschi, D. Unpublished results.

Table 3. Selected Bond Lengths (Å) and Angles (deg) for $KFe_3(OCH_3)_7(dbm)_3 \cdot 4CH_3OH$[a]

O(1)−Fe(1)	2.148(2)	O(2)−Fe(1)	2.028(2)
O(4)−Fe(1)	1.989(2)	O(5)−Fe(1)	2.038(2)
O(6)−Fe(1)	2.008(2)	O(11)−Fe(1)	1.884(3)
O(1)−Fe(2)	2.133(2)	O(2)−Fe(2)	1.998(2)
O(3)−Fe(2)	2.005(2)	O(7)−Fe(2)	2.033(2)
O(8)−Fe(2)	2.023(2)	O(12)−Fe(2)	1.897(2)
O(1)−Fe(3)	2.151(2)	O(3)−Fe(3)	2.001(2)
O(4)−Fe(3)	2.007(2)	O(9)−Fe(3)	2.039(3)
O(10)−Fe(3)	2.022(2)	O(13)−Fe(3)	1.877(2)
C(1)−O(1)	1.437(3)	C(2)−O(2)	1.433(5)
C(3)−O(3)	1.423(3)	C(4)−O(4)	1.434(4)
C(5)−O(5)	1.275(3)	C(7)−O(6)	1.274(3)
C(8)−O(7)	1.275(4)	C(10)−O(8)	1.275(4)
C(11)−O(9)	1.273(4)	C(13)−O(10)	1.278(4)
C(14)−O(11)	1.406(5)	C(15)−O(12)	1.395(5)
C(16)−O(13)	1.398(6)	C(17)−O(14)	1.391(5)
C(18)−O(15)	1.394(7)	C(19)−O(16)	1.401(5)
Cs−Os	1.418(8)	K−O(2)	2.821(2)
K−O(3)	2.905(2)	K−O(4)	2.974(2)
K−O(14)	2.668(3)	K−O(15)	2.607(4)
K−O(16)	2.744(2)	K−Os	3.242(4)
HOs−Os	0.83(5)	HO(14)−O(14)	0.73(4)
HO(15)−O(15)	0.74(4)		

O(2)−Fe(1)−O(1)	76.64(8)	O(4)−Fe(1)−O(1)	76.93(9)
O(5)−Fe(1)−O(1)	96.74(8)	O(6)−Fe(1)−O(1)	90.93(9)
O(11)−Fe(1)−O(1)	166.84(7)	O(4)−Fe(1)−O(2)	93.9(1)
O(5)−Fe(1)−O(2)	170.6(1)	O(6)−Fe(1)−O(2)	88.4(1)
O(11)−Fe(1)−O(2)	93.7(1)	O(5)−Fe(1)−O(4)	91.0(1)
O(6)−Fe(1)−O(4)	166.7(1)	O(11)−Fe(1)−O(4)	95.1(1)
O(6)−Fe(1)−O(5)	85.1(1)	O(11)−Fe(1)−O(5)	93.8(1)
O(11)−Fe(1)−O(6)	97.8(1)	O(2)−Fe(2)−O(1)	77.63(8)
O(3)−Fe(2)−O(1)	76.86(7)	O(7)−Fe(2)−O(1)	97.98(7)
O(8)−Fe(2)−O(1)	89.95(8)	O(12)−Fe(2)−O(1)	168.59(9)
O(3)−Fe(2)−O(2)	91.3(1)	O(7)−Fe(2)−O(2)	89.6(1)
O(8)−Fe(2)−O(2)	165.5(1)	O(7)−Fe(2)−O(3)	174.4(1)
O(12)−Fe(2)−O(2)	96.4(1)	O(8)−Fe(2)−O(3)	93.0(1)
O(8)−Fe(2)−O(7)	84.8(1)	O(12)−Fe(2)−O(3)	93.7(1)
O(12)−Fe(2)−O(7)	91.7(1)	O(12)−Fe(2)−O(8)	97.0(1)
O(3)−Fe(3)−O(1)	76.53(7)	O(4)−Fe(3)−O(1)	76.49(8)
O(9)−Fe(3)−O(1)	97.13(9)	O(10)−Fe(3)−O(1)	92.40(8)
O(13)−Fe(3)−O(1)	166.8(1)	O(4)−Fe(3)−O(3)	92.8(1)
O(9)−Fe(3)−O(3)	88.9(1)	O(10)−Fe(3)−O(3)	166.6(1)
O(13)−Fe(3)−O(3)	96.2(1)	O(9)−Fe(3)−O(4)	172.8(1)
O(10)−Fe(3)−O(4)	91.9(1)	O(13)−Fe(3)−O(4)	93.1(1)
O(10)−Fe(3)−O(9)	84.9(1)	O(13)−Fe(3)−O(9)	93.7(1)
O(13)−Fe(3)−O(10)	96.0(1)	Fe(2)−O(1)−Fe(1)	98.40(9)
Fe(1)−O(1)−Fe(3)	98.00(8)	Fe(2)−O(1)−Fe(3)	98.39(6)
C(1)−O(1)−Fe(1)	118.6(2)	C(1)−O(1)−Fe(2)	119.8(2)
C(1)−O(1)−Fe(3)	119.2(2)	Fe(2)−O(2)−Fe(1)	107.2(1)
C(2)−O(2)−Fe(1)	118.7(2)	C(2)−O(2)−Fe(2)	121.5(2)
Fe(3)−O(3)−Fe(2)	108.0(1)	C(3)−O(3)−Fe(2)	122.4(2)
C(3)−O(3)−Fe(3)	121.3(2)	Fe(3)−O(4)−Fe(1)	108.6(1)
C(4)−O(4)−Fe(1)	120.1(2)	C(4)−O(4)−Fe(3)	121.1(2)
C(5)−O(5)−Fe(1)	129.7(2)	C(7)−O(6)−Fe(1)	131.5(2)
C(8)−O(7)−Fe(2)	129.7(2)	C(10)−O(8)−Fe(2)	131.1(2)
C(11)−O(9)−Fe(3)	127.9(2)	C(13)−O(10)−Fe(3)	128.7(2)
C(14)−O(11)−Fe(1)	125.3(2)	C(15)−O(12)−Fe(2)	126.1(2)
C(16)−O(13)−Fe(3)	130.8(2)	O(15)−K−O(14)	105.0(1)
O(15)−K−O(16)	111.6(1)	O(15)−K−O(2)	87.58(8)
O(15)−K−O(3)	137.82(7)	O(15)−K−O(4)	82.33(8)
O(15)−K−Os	115.5(1)	O(14)−K−O(16)	88.04(9)
O(14)−K−O(2)	133.84(7)	O(14)−K−O(3)	83.77(8)
O(14)−K−O(4)	76.82(6)	O(14)−K−Os	130.08(9)
O(16)−K−O(2)	128.84(9)	O(16)−K−O(3)	109.87(9)
O(16)−K−O(4)	161.9(1)	O(16)−K−Os	51.25(9)
O(2)−K−O(3)	59.97(7)	O(2)−K−O(4)	60.80(6)
O(2)−K−Os	77.60(6)	O(3)−K−O(4)	59.18(5)
O(3)−K−Os	85.05(9)	O(4)−K−Os	134.39(7)
C(17)−O(14)−HO(14)	101(3)	C(18)−O(15)−HO(15)	119(5)
Cs−Os−HOs	109(4)		

[a] Numbers in parentheses are errors in the last significant digit.

$[Fe_3(OCH_3)_7(dbm)_3]^-$ core described so far approaches the C_{3v} point symmetry if the nonplanarity of the *dbm* moieties is neglected. However, significant distortions from the above idealized symmetry show up on careful inspection of the metrical parameters reported in Table 3 and sketched in structure **I**. Two of the Fe−O(1) bond distances are essentially equal to each other [O(1)−Fe(1) = 2.148(2) Å, O(1)−Fe(3) = 2.151(2) Å] whereas the third one is significantly shorter [O(1)−Fe(2) = 2.133(2) Å]. Some distortions affect the μ_2-OCH_3 bridges as well. While O(3) bridges in a symmetrical fashion, the O(3)−Fe(3) and O(3)−Fe(2) distances being equal within experimental error, O(2) and, to a lower extent, O(4) have

Table 4. Selected Nonbonded Distances (Å) and Angles (deg) for $KFe_3(OCH_3)_7(dbm)_3 \cdot CH_3OH$[a]

Fe(1)−Fe(2)	3.241(1)	Fe(1)−Fe(3)	3.244(1)
Fe(2)−Fe(3)	3.242(1)	Fe(1)−K	3.741(1)
Fe(2)−K	3.766(1)	Fe(3)−K	3.837(1)
Fe(2)−Fe(1)−Fe(3)	59.99(1)	Fe(1)−Fe(2)−Fe(3)	60.06(1)
Fe(2)−Fe(3)−Fe(1)	59.95(1)	Fe(2)−Fe(1)−K	64.82(2)
Fe(3)−Fe(1)−K	66.20(2)	Fe(1)−Fe(2)−K	64.03(1)
Fe(3)−Fe(2)−K	65.91(2)	Fe(2)−Fe(3)−K	63.62(2)
Fe(1)−Fe(3)−K	63.13(2)	Fe(1)−K−Fe(2)	51.15(1)
Fe(1)−K−Fe(3)	50.67(1)	Fe(2)−K−Fe(3)	50.47(1)

[a] Numbers in parentheses are estimated standard deviations in the last significant digit.

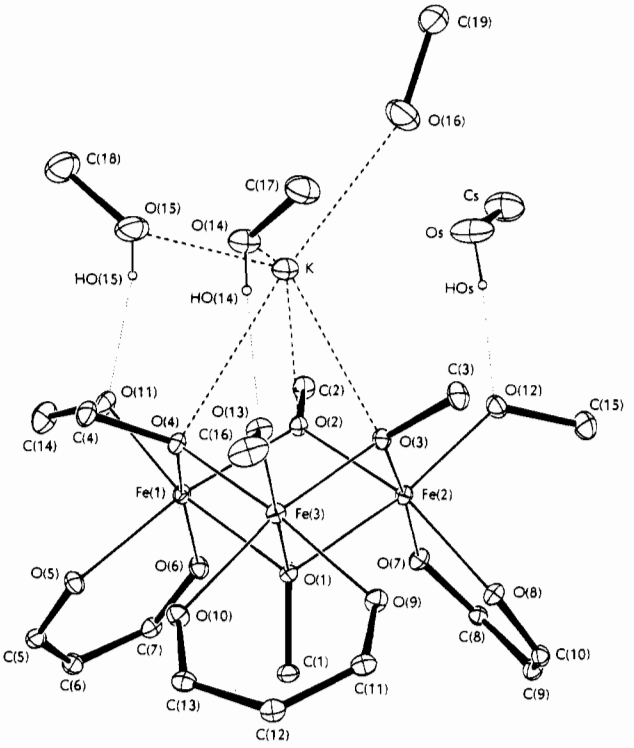

Figure 1. ORTEP view of compound **7**. The carbon atoms of the phenyl rings of the *dbm* ligands and all hydrogen atoms except for HO(14), HO(15) and HOs have been omitted for clarity. Thermal ellipsoids enclose 20% probability.

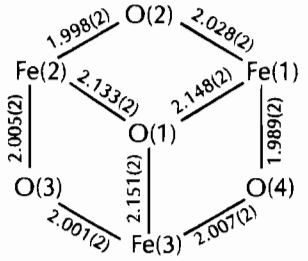

I

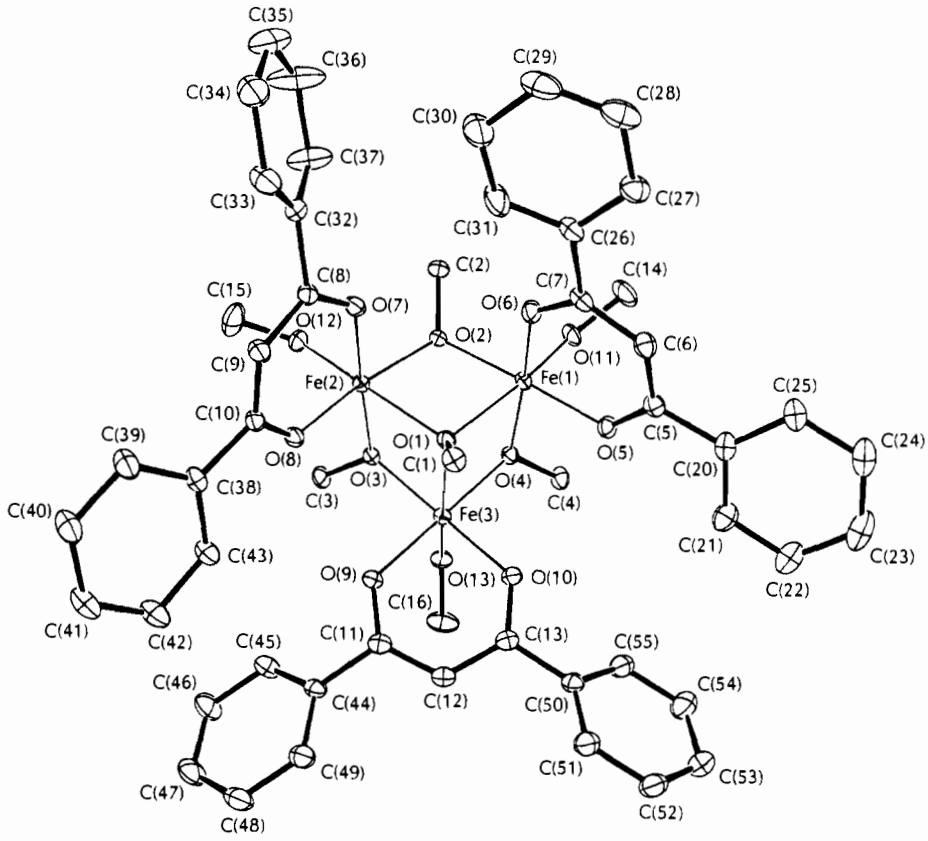

Figure 2. ORTEP plot of the $Fe_3(OCH_3)_7(dbm)_3^-$ moiety of compoud **7** as viewed along its virtual C_3 axis. Hydrogen atoms have been omitted for clarity. Thermal ellipsoids enclose 20% probability.

significantly different bond distances with the iron atoms of each appropriate pair. Small differences are also found in the bond distances of each iron center with the oxygen from the corresponding terminal methoxide ligand. Namely, O(12)−Fe(2) [1.897(2) Å] is longer than the remaining two separations, which average 1.88 Å.

All the above observations can be satisfactorily rationalized by looking at the arrangement of the potassium ion and of the methanol molecules with respect to the $[Fe_3(OCH_3)_7(dbm)_3]^-$ core. The iron centers and the potassium ion in **7** are found at the vertices of a distorted tetrahedron whose metrical parameters are summarized in Table 4. The potassium ion occupies the molecular hemicavity which results from the arrangement of the iron−oxygen framework of the trinuclear core and is coordinated by the three oxygen donors of the μ_2-methoxides. The K−O(2) separation [2.821(2) Å] is significantly shorter than K−O(3) [2.905(2) Å] and K−O(4) [2.974(2) Å], which partially explains the lengthening of the O(2)−Fe(1) distance. The methanol molecules are asymmetrically arranged. Two of them coordinate the potassium ion and are hydrogen-bonded to O(11) and O(13) of the monodentate methoxides with essentially equal O···O separations. The geometrical parameters of hydrogen-bond interactions are given in Table 5. A third solvent molecule is coordinated to the potassium ion only. The last methanol molecule is loosely bound to the latter, while having a strong hydrogen bond with O(12), a situation which may be reflected in the long O(12)−Fe(2) separation. The shortening of the O(1)−Fe(2) distance then follows as a *trans* effect. Though the hydrogen atom attached to O(16) could not be located in ΔF maps, the O(16)−Os separation [2.628(5) Å] suggests that a hydrogen bond may be present between O(16) and Os as well.

The triiron(III)-methoxide core of complex **7** is an example of a 6-metallacrown-3 structure type in which the six-membered ring of iron(III) and oxygen atoms Fe(1)−O(2)−Fe(2)−O(3)−Fe(3)−O(4) binds the potassium ion on one side. Interestingly, the hexairon(III)−methoxide cluster $[MFe_6(OCH_3)_{12}(dbm)_6]\cdot 12CH_3OH\cdot CHCl_3$ (M = Na, Li) (**9**) displaying the related 12-metallacrown-6 structure type and harboring the sodium or lithium ion in the center has been recently isolated.[18,19] Examples of the 9-metallacrown-3[20] and 12-metallacrown-4[21] structure types are also available.

Table 5. Hydrogen-Bond Distances (Å) and Angles (deg) for $KFe_3(OCH_3)_7(dbm)_3\cdot 4CH_3OH$[a]

HO(14)···O(13	1.91(4)	O(14)···O(13)	2.638(3)
O(14)-HO(14)···O(13)	171(5)		
HO(15)···O(11)	1.92(4)	O(15)···O(11)	2.642(3)
O(15)-HO(15)···O(11)	167(6)		
HOs···O(12)	1.78(5)	Os···O(12)	2.599(4)
Os-HOs···O(12)	170(5)		
O(16)···Os	2.628(5)		

[a] Numbers in parentheses are estimated standard deviations in the last significant digit.

Compound **7** is structurally related to a number of poly-iron(III)−oxo aggregates studied in recent years. Complexes **3**−**6** all contain triangular arrays of iron atoms with μ_3-OCH_3 ligands. Noticeably, the $[Fe_3(\mu_3\text{-}OCH_3)(\mu_2\text{-}OCH_3)_3(OCH_3)_3(dbm)_3]^-$ core observed in **7** shows striking similarities with the $Fe_3(\mu_3\text{-}OCH_3)_4(CH_3OH)_3(L)_3$ fragments which can be individuated in **5** and **6** (L = *dbm*, *dpm*, respectively). Indeed, the two latter compounds can be formally constructed from **7** by replacing the $K(CH_3OH)_4$ unit with a $Fe(CH_3OH)(L)$ unit and transforming the μ_2-OCH_3 and monodentate methoxides into μ_3-OCH_3 and monodentate methanol molecules, respectively.

(20) Lah, M. S.; Kirk, M. L.; Hatfield, W.; Pecoraro, V. L. *J. Chem. Soc., Chem. Commun.* **1989**, 1606.
(21) Lah, M. S.; Pecoraro, V. L. *J. Am. Chem. Soc.* **1989**, *111*, 7258.

Similar $Fe_3(\mu_3\text{-}OR)_2(\mu_2\text{-}OR)_2$ fragments are also present in the complex $Fe_4(dbsq)_4(dbcat)_4$ (**10**).[6,22]

Several structural analogies with the three hexanuclear μ_6-oxo bridged clusters known so far[23−25] are also apparent. Their $Fe_6(\mu_6\text{-}O)$ core can be imagined to derive from the fusion of two $Fe_3(\mu_3\text{-}OCH_3)$ units, with suppression of the methyl groups and transformation of the methoxide oxygen atom into a μ_6-oxo ligand. Interestingly, the topology of the K atom in **7** is strictly similar to that of the Na counterions in $Na_2Fe_6(\mu_6\text{-}O)(OCH_3)_{18}\cdot 6CH_3OH$ (**11**),[23] each alkali-metal ion being coordinated, in this second case, by three oxygen donors from μ_2-OCH_3 ligands in correspondence of a triangular face of the metal octahedron.

In the hexairon(III) cluster $Fe_6(O)_2(OCH_3)_{12}(tren)_2(CF_3SO_3)_2\cdot 2CH_3OH$ (**12**),[6,26] $Fe_3(\mu_4\text{-}O)(OCH_3)_3$ and $Fe_3(\mu_4\text{-}O)_2(OCH_3)_2$ moieties can be easily recognized which bear structural resemblance to the core of **7**.

A comparison with other structurally characterized triiron(III) complexes is also instructive. Most of them exhibit the well-known symmetric μ_3-oxo-centered structure typical of "basic iron carboxylates".[27] The central μ_3-oxide ligand is coplanar to the three iron(III) ions which are further bridged by carboxylate or sulfate ligands.[28] Asymmetric μ_3-oxo-centered[29] and linear[30] trinuclear iron(III) complexes have also been reported.

In **7** the structure is more similar to that postulated for the active sites of [3Fe4S] proteins.[31] The possible formation of heterometal clusters $[MFe_3S_4]^{+,2+}$ [M = Co(II), Zn(II)] in the active sites of *Desulfovibrio gigas* Fd II has been demonstrated. Structurally, they are similar to the $[KFe_3(\mu_3\text{-}OCH_3)(\mu_2\text{-}OCH_3)_3]$ core of compound **7**.

The conversion of the cubane mixed-valent $[Fe_4S_4]^{2+}$ (**13**) into $[Fe_3S_4]^0$ (**14**) and $[Fe_3S_4]^+$ (**15**) formally proceeds by removal of an iron(II) ion and a subsequent one-electron oxidation step, respectively. However, as shown by cyclic voltammetry experiments of both 1,2-dichloroethane and acetonitrile solutions, **7** does not undergo any reversible redox process in the range −1.5/+1.5 V *vs* Fc+/Fc.

Trinuclear complexes of the early-transition elements with sulfide or oxide bridges and a similar overall structure are also known.[32]

Structural Relevance to Iron Oxides and Hydroxides. Several polyiron(II,III) clusters exhibiting a *closest-packing (cp)*[33] of oxygen atoms have been isolated in recent years. Two such layers of oxygen atoms from hydroxide, oxide, alkoxide, or phenoxide ligands are found in the cores of the complexes **1**, **2**, and **9** and of the heptairon(II) cluster $Fe^{II}_7(OCH_3)_6(OPh)_6(CH_3CN)_{12}^{2+}$ (**16**),[34] all of which display the CdI_2-type structure.[33] Similar *cp* layered structures have been recently observed in the cores of two nickel(II) clusters with siloxanolate ligands.[35]

In complex **7**, the 13 oxygen atoms in the first coordination sphere of iron(III) ions are arranged in two essentially parallel layers. Atoms O(1), O(5), O(6), O(7), O(8), O(9), and O(10) show average deviations of 0.14 Å from the best plane through them (plane *a*). With respect to the idealized geometry of a hexagonal net, plane *a* displays significant distortions, which arise from the constraints imposed by the chelating *dbm* ligands (Chart 1a). In fact, the shortest distances between oxygen atoms *from the same dbm ligand* and *from different dbm ligands* average 2.738(3) and 3.37(9) Å, respectively, whereas O(*i*)−O(1) separations (i = 5, 6, ..., 10) average 3.05(9) Å. Less evident distortions affect the mean plane through O(2), O(3), O(4), O(11), O(12) and O(13) (plane *b*, see Chart 1b), in which O···O separations average 2.87(3) Å. However, larger deviations of the atoms from the best plane are present (0.23 Å, after averaging). Planes *a* and *b* and the mean plane through the iron atoms (plane *c*) are parallel within 0.5°. Planes *a* and *b* are also almost equidistant from the plane through the metals (1.20 and 1.08 Å, respectively). A third incomplete layer of oxygen atoms can be envisaged in complex **7**. It comprises O(14), O(15) and Os (plane *d*), with O···O distances larger than 4 Å, and is found to be parallel to planes *a*−*c* within 1.1°. The potassium ion lies very close to plane *d* (0.50 Å) whereas its distance from plane *b* is much larger (2.20 Å). In Chart 1c the three layers of oxygen atoms described by planes *a*, *b*, and *d* are depicted. O(16) is also indicated, but it must be remembered that O(16) lies quite far from plane *d*. It is seen that the large ionic radius of potassium and hydrogen bond interactions (marked by thin dotted lines) result in dramatic distortions of the arrangement of oxygen atoms of plane *d* with respect to the idealized positions of a *cubic-closest-packing* (*ccp*),[33] which are indicated by cross hairs. A distorted *ccp* of oxygen atoms has indeed been observed in complexes **3**−**6** and in the hexanuclear μ_6-oxo-centered clusters.[23−25] It is noteworthy that the structure of these *molecular* aggregates has so much in common with the three-dimensional lattices of metal oxides displaying a *ccp* of oxygen atoms, such as NiO, FeO and γ-Fe_2O_3. The related *hexagonal-closest-packing* (*hcp*) is found in α-Fe_2O_3. α-FeO(OH) (göthite) and γ-FeO(OH) (lepidocrocite) contain *cp* layers of oxygen atoms as well.[5,33] The O···O separations within

(22) Boone, S. R.; Purser, G. H.; Chang, H.-R.; Lowery, M. D.; Hendrickson, D. N.; Pierpont, C. G. *J. Am. Chem. Soc.* **1989**, *111*, 2292.
(23) Hegetschweiler, K.; Schmalle, H. W.; Streit, H. M.; Schneider, W. *Inorg. Chem.* **1990**, *29*, 3625.
(24) Hegetschweiler, K.; Schmalle, H. W.; Streit, H. M.; Gramlich, V.; Hund, H. U.; Erni, I. *Inorg. Chem.* **1992**, *31*, 1299.
(25) Cornia, A.; Gatteschi, D.; Hausherr, L.; Hegetschweiler, K. Unpublished results.
(26) Nair, V. S.; Hagen, K. S. *Inorg. Chem.* **1992**, *31*, 4048.
(27) Scheurer-Kestner, M. *Ann. Chim. Phys., Ser. 3*, **1861**, *63*, 422. Weinland, R. F.; Hohn, A. *Z. Anorg. Chem.* **1926**, *152*, 1. Welo, L. A. *Philos. Mag. S7* **1928**, *6*, 481. Earnshaw, A.; Figgis, B. N.; Lewis, J. *J. Chem. Soc. A* **1966**, 1656.
(28) Holt, E. M.; Holt, S. L.; Tucker, W. F.; Asplund, R. O.; Watson, K. J. *J. Am. Chem. Soc.* **1974**, *96*, 2621. Heald, S. M.; Stearn, E. A.; Bunker, B.; Holt, E. M.; Holt, S. L. *J. Am. Chem. Soc.* **1979**, *101*, 67. Holt, E. M.; Holt, S. L.; Alcock, N. W. *Cryst. Struct. Commun.* **1982**, *11*, 505. Dziobkowski, C. T.; Wrobleski, J. T.; Brown, D. B. *Inorg. Chem.* **1981**, *20*, 671. Uemura, S.; Spencer, A.; Wilkinson, G. *J. Chem. Soc., Dalton Trans.* **1973**, 2565. Catterick, J.; Thornton, P.; Fitzsimmons, B. W. *J. Chem. Soc., Dalton Trans.* **1977**, 1420. Catterick, J.; Thornton, P. *Adv. Inorg. Chem. Radiochem.* **1977**, *20*, 291. Cotton, F. A.; Wilkinson, G. *Advanced Inorganic Chemistry*; Wiley: New York, 1980; pp 154−155. Thich, J. A.; Toby, B. H.; Powers, D. A.; Potenza, J. A.; Schugar, H. J. *Inorg. Chem.* **1981**, *20*, 3314. Giacovazzo, G.; Scordari, F.; Menchetti, S. *Acta Crystallogr.* **1975**, *B31*, 2171. Cannon, R. D.; White, R. P. *Progr. Inorg. Chem.* **1988**, *36*, 195.
(29) Gorun, S. M; Lippard, S. J. *J. Am. Chem. Soc.* **1985**, *107*, 4568. Gorun, S. M.; Papaefthymiou, G. C.; Frankel, R. B.; Lippard, S. J. *J. Am. Chem. Soc.* **1987**, *109*, 4244.
(30) Kitajima, N.; Amagai, H.; Tamura, N.; Ito, M.; Moro-oka, Y.; Heerwegh, K. Penicaud, A.; Mathur, R.; Reed, C. A.; Boyd, P. D. W. *Inorg. Chem.* **1993**, *32*, 3583.
(31) Berg, J. M.; Holm, R. H. In *Iron Sulfur Proteins*; Spiro, T. G., Ed; John Wiley and Sons: New York, 1982; Vol. 4. Holm, R. H.; Ciurli, S.; Weigel, J. A. *Prog. Inorg. Chem.* **1990**, *38*, 1.
(32) Müller, A.; Jostes, R.; Cotton, F. A. *Angew. Chem., Int. Ed. Engl.* **1980**, *19*, 875 and references therein.
(33) Wells, A. F. *Structural Inorganic Chemistry*, 5th ed.; Clarendon Press: Oxford, England, 1984; p 258.
(34) Nair, V. S.; Kitaygorodskiy, A.; Hagen, K. S. Presented at the 206th National Meeting of the American Chemical Society, Chicago, IL, 1993.
(35) Levitsky, M. M.; Shchegolikhina, O.; Zhdanov, A. A.; Igonin, V. A.; Ovchinnikov, Yu. E.; Shklover, V. E.; Struchkov, Yu. T. *J. Organomet. Chem.* **1991**, *401*, 199. Igonin,V. A.; Lindeman, S. V.; Potekhin, K. A.; Shklover, V. E.; Struchkov, Yu. T.; Shchegolikhina, O.; Zhdanov, A. A.; Razumovskaya, I. V. *Organomet. Chem. USSR* **1991**, *4*, 383.

Chart 1

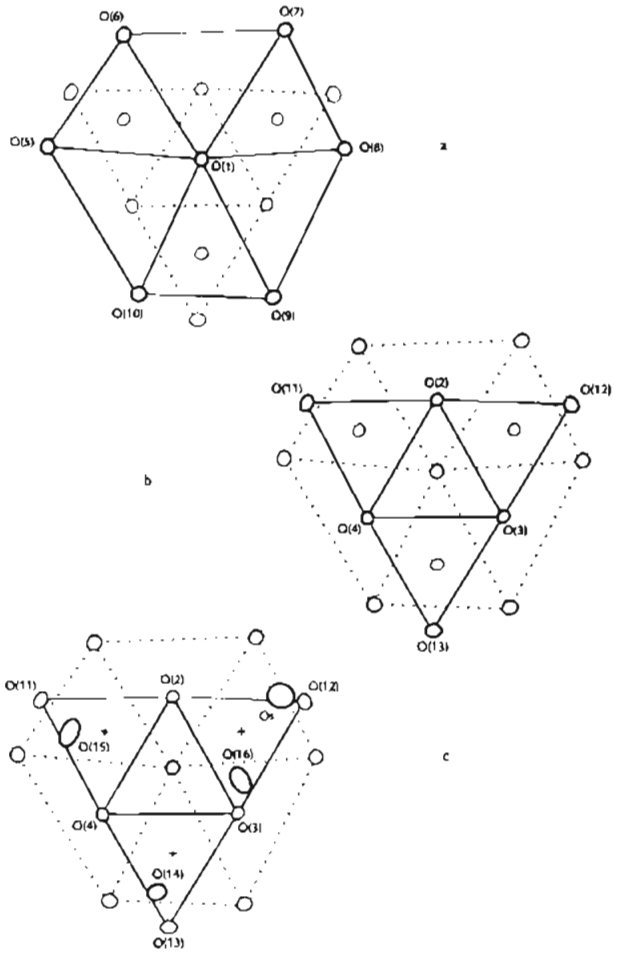

planes *a* and *b* in complex **7** are to be compared with the values found in FeO (3.04 Å), in α-Fe_2O_3 (2.70−3.04 Å) and in α-FeO(OH) (2.74−2.84 Å).

Magnetic Behavior. The measured molar magnetic susceptibility of **7** in a field of 1 T is plotted in Figure 3 as a function of temperature. The insert shows the temperature dependence of the χT product. The susceptibility (0.0345 emu·mol^{-1} at 270 K) increases steadily with decreasing temperature, reaching 0.2100 emu·mol^{-1} at 2.2 K. The room-temperature χT product (8.93 emu·K·mol^{-1}) is appreciably lower than expected for three uncoupled $S = {}^5/_2$ spins (13.13 emu·K·mol^{-1}). When the sample is cooled down, χT decreases continuously and does not extrapolate to zero as temperature approaches 0 K, as expected for three $S = {}^5/_2$ spins ($\chi T = 0.46$ emu·K·mol^{-1} at 2.2 K). The system obeys the Curie−Weiss law down to about 60 K, with $C = 13.48$ emu·K·mol^{-1} and $\Theta = -137.5$ K.

A C_{2v} point-group symmetry was assumed for the triiron complex and a spin-only Heisenberg−Dirac−VanVleck (HDVV) Hamiltonian formalism was adopted to reproduce the observed magnetic behavior.

$$\mathbf{H}_{HDVV} = J(\mathbf{S}_1\cdot\mathbf{S}_2 + \mathbf{S}_1\cdot\mathbf{S}_3) + J'\mathbf{S}_2\cdot\mathbf{S}_3 \qquad (1)$$

The usual Kambe[36] vector-coupling approach gives the energies of the spin states as functions of the exchange integrals J and J'.

$$E(S_T, S_{23}) = [J/2]S_T(S_T + 1) + [(J' - J)/2]S_{23}(S_{23} + 1) \qquad (2)$$

(36) Kambe, K. *J. Phys. Soc. Jpn.* **1950**, *5*, 48.

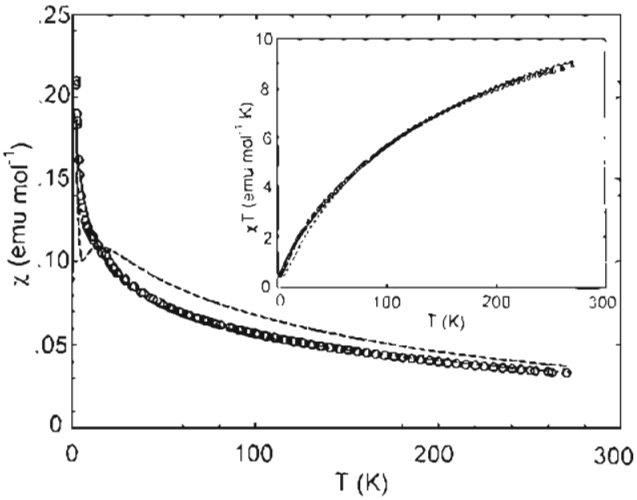

Figure 3. Temperature dependence of χ and χT for compound **7** in an applied field of 1 T. The calculated curves for $g = 2.0$, $J = J' = 8.7$ cm^{-1} (dashed line) and for $g = 2.0$, $J = 10.6$ cm^{-1}, $J' = 15.3$ cm^{-1} (solid line) are also shown.

where $\mathbf{S}_{23} = \mathbf{S}_2 + \mathbf{S}_3$ and $\mathbf{S}_T = \mathbf{S}_1 + \mathbf{S}_{23}$. No satisfactory fitting of the experimental susceptibility could be obtained setting $J' = J$ (*i.e.* assuming C_{3v} point-group symmetry). In fact, the J value which gives an acceptable fitting to χT, $J = 8.7(1)$ cm^{-1}, requires a maximum in χ at about 20 K which is not experimentally observed (Figure 3). Relaxation of the condition $J' = J$ was then allowed. This has an important physical consequence when J', $J > 0$: it partially removes the 4-fold degeneracy of the spin ground state of the system in zero field. In fact, when $J' = J$, the energy of the spin states does not depend on the intermediate spin quantum number S_{23} [see (2)] and for $J > 0$ the ground state is given by two degenerate spin doublets, arising from $S_{23} = 2$ and $S_{23} = 3$. However, when $J' \neq J$, the energy of the spin states does depend on S_{23} and the energy gap between the two doublets is given by

$$|E({}^1/_2, 3) - E({}^1/_2, 2)| = 3|J' - J| \qquad (3)$$

A net improvement in the quality of the fit was achieved (Figure 3). However, two distinct minima are present on the relative-error surface, corresponding to the two sets $J = 10.6(1)$, $J' = 15.3(2)$ cm^{-1} (*a*) and $J = 12.9(2)$, $J' = 9.7(1)$ cm^{-1} (*b*). In the resulting picture of the spin states, the energy gap between the two lowest-lying doublets is 14.1 and 9.6 cm^{-1} for sets *a* and *b*, respectively. As a consequence of the reorganization of the spin states with respect to the C_{3v} approximation, the first excited multiplet lies 6.5 cm^{-1} above the ground spin doublet and is characterized by $S_{23} = 1$, $S_T = 3/2$ for set *a* and $S_{23} = 4$, $S_T = 3/2$ for set *b*.

The estimated magnitude of the exchange integrals, J and J', compares well with a number of observations on alkoxo-bridged polyiron(III) complexes. Current treatments of magnetic-exchange interactions between iron(III) centers involving oxygen bridging atoms emphasize the role of the coupling distance P, defined as half of the shortest super-exchange pathway between two iron(III) ions, in determining the antiferromagnetic contributions to magnetic coupling. In multiply-bridged diiron(III) units, an *inverse exponential* dependence of J upon P has been established empirically.[37] Possible super-exchange pathways in compound **7** involve the O(1), O(2), O(3), and O(4) oxygen atoms from bridging methoxide ligands. In structure **I**, we

(37) Gorun, S. M.; Lippard, S. J. *Inorg. Chem.* **1991**, *30*, 1625. Turowski, P. N.; Armstrong, W. H.; Roth, M. E.; Lippard, S. J. *J. Am. Chem. Soc.* **1990**, *112*, 681.

report a sketch of the $Fe_3(O)_4$ skeleton from which the length of the various superexchange pathways can be calculated. It is easily seen that for each iron−iron interaction the *shortest pathway* invariably involves oxygens from μ_2-OCH_3 ligands. Use of the average iron−iron coupling distance (2.005 Å) in conjunction with the equation reported in ref 37 leads to $J_{av} = 16.6\ cm^{-1}$, which is of the right order of magnitude. Unfortunately, it is not possible to draw a conclusion as to which set of coupling constants is more likely to be the right one. Judging from the metrical parameters of the $Fe_3(O)_4$ skeleton, the Fe(1)−Fe(2) magnetic interaction through O(2) should be weaker than the other two.

The large structural differences between "basic" carboxylates and complex **7** have one major consequence: for iron(III) "basic" carboxylates typical J values resulting from the equilateral-triangle model ($60\ cm^{-1}$)[29] are almost 1 order of magnitude larger than for complex **7** ($8.7\ cm^{-1}$). In fact, though the average iron−iron separation is smaller in complex **7** than in "basic carboxylates" (3.24 *vs* 3.32 Å), in the latter the iron−iron coupling distance, which involves the central μ_3-oxide ligand, is shorter than in complex **7** (1.92 *vs* 2.00 Å). As a result, while the highest spin states of iron(III) "basic" carboxylates are not significantly populated at room-temperature, the energy of the $S = {}^{15}/_2$ manifold of cluster **7** is comparable to the thermal energy at room-temperature. Moreover, according to the equilateral-triangle model the first excited multiplet ($S_T = {}^3/_2$) in **7** lies approximately 13 cm^{-1} above the ground state, whereas in "basic" carboxylates the energy gap can be as large as 50 cm^{-1} and the ground state is therefore much more "isolated".

The results obtained by the application of HDVV Hamiltonians to the interpretation of the magnetic data of compound **7** suggest that, with respect to the predictions of C_{3v} HDVV Hamiltonian, a *complete* reorganization of the spin states is necessary in order to reproduce the observed magnetic behavior. Within the HDVV formalism this can be successfully achieved by taking into account distortions from the idealized trigonal symmetry. The same situation is commonly encountered in triiron(III) μ_3-oxo-centered "basic" carboxylates, in which case it does *not* seem to arise merely from structural inequivalency of the three exchange pathways.

An alternative explanation for the magnetic behavior of **7** retaining an idealized trigonal symmetry is the presence of non-Heisenberg exchange contributions. In triangular arrays of antiferromagnetically-coupled half-integer spins with trigonal symmetry the two $S = {}^1/_2$ states, which can be referred to as ^2E, are split by spin-orbit interaction. In the spin Hamiltonian approach this corresponds to the introduction of antisymmetric exchange (AS) terms.[38,39] More generally, AS- and Heisenberg-exchange contributions sum up in determining the splitting of the ^2E state in a distorted system. A convenient Hamiltonian for a C_{2v}-symmetry array of three interacting spins in a magnetic field H, assuming an isotropic g factor and including AS-exchange interactions, has the form

$$\mathbf{H} = \mathbf{H}_{HDVV} + \mathbf{H}_{AS} + \mathbf{H}_Z = J(\mathbf{S}_1\cdot\mathbf{S}_2 + \mathbf{S}_1\cdot\mathbf{S}_3) + J'\mathbf{S}_2\cdot\mathbf{S}_3 + \mathbf{G}[(\mathbf{S}_1 \times \mathbf{S}_2) + (\mathbf{S}_2 \times \mathbf{S}_3) + (\mathbf{S}_3 \times \mathbf{S}_1)] + g\mu_B\mathbf{H}\cdot\mathbf{S}_T \quad (4)$$

where **G** is the vector of antisymmetric exchange[38] and the other symbols have their usual meaning. In the following we will set $G_x = G_y = 0$, which may be expected to hold if the distortions from C_{3v} symmetry are small, and we will assume that the leading contribution to **H** comes from the Heisenberg exchange terms. For $S = {}^5/_2$ spins the energy of the four magnetic sublevels of the ground state, as resulting from a first-order perturbation treatment,[39] is given by

$$E(H) = \pm 0.5[\Delta^2 + (g\mu_B H)^2 \pm 2g\mu_B H\,(\delta^2 + D^2\cos^2\Theta)^{1/2}]^{1/2} \quad (5)$$

where $H = |\mathbf{H}|$, $D = D_z = 9(3)^{1/2}G_z$, $\delta = 3(J' - J)$, $\Delta^2 = \delta^2 + D^2$ and Θ is the angle between the field and the z axis, which is normal to the plane of the cluster.[38,39]

The parameter Δ thus measures the splitting of the magnetic sublevels in zero field (Figure 4).

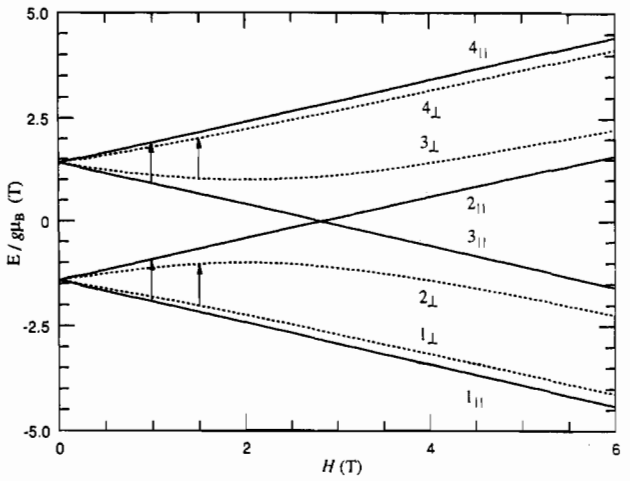

Figure 4. Field dependence of the eigenvalues of Hamiltonian (4), with the assumptions explained in the text and $\delta/g\mu_B = D/g\mu_B = 2$ T ($g = 2.0$). The arrows show the transitions which are believed to be responsible of the observed EPR signals in compound **7** and **17**. The resonance fields are not to scale.

We tried to apply the above formulas to the ground state of complex **7**, while retaining the condition $J = J'$. However, no net improvement of the quality of the fit resulted. This confirms that the *overall* picture of the spin levels arising from the C_{3v} HDVV model is incorrect and that the discrepancies do not merely depend on the splitting of the ground state.

X-Band EPR spectra recorded on powdered samples provide useful information about the relative importance of AS- and Heisenberg-exchange contributions to the splitting of the ^2E state. At room temperature, a single broad line is observed at $g \approx 2$. On cooling down the sample, the intensity of the signal increases gradually and at liquid helium temperature an anisotropic line is present at $g_{eff} = 1.89$ ($\Delta H = 575$ G) (Figure 5). Since the HDVV model predicts that an isotropic EPR line should be observed at the single-ion g value [$g = 2.00$ for iron(III)], irrespective of the geometry of the cluster,[38] non-Heisenberg contributions must be present.

Comparison with the X-band EPR spectra of $[Fe_3O(CH_3CO_2)_6(H_2O)_3]Cl\cdot 4H_2O$ (**17**)[38] may be instructive. Two overlapping lines at $g_{eff} \approx 2$ and 1.6−1.4 are observed on polycrystalline samples at liquid-helium temperature. They are believed to arise from "parallel" and "perpendicular" transitions involving the four magnetic sublevel of ^2E parentage (see Figure 4). The resonance fields calculated by (5) are

$$H_{\parallel} = (h\nu/g\mu_B) \quad (6)$$

$$H_{\perp} = (h\nu/g\mu_B)\{[\Delta^2 - (h\nu)^2]/[\delta^2 - (h\nu)^2]\}^{1/2} \quad (7)$$

(38) Rakitin, Yu. V.; Yablokov, Yu. V.; Zelentsov, V. V. *J. Magn. Reson.* **1981**, *43*, 288.
(39) Tsukerblat, B. S.; Belinskii, M. I.; Fainzil'berg, V. E. *Sov. Sci. Rev. B. Chem.* **1987**, *9*, 337 and references therein.

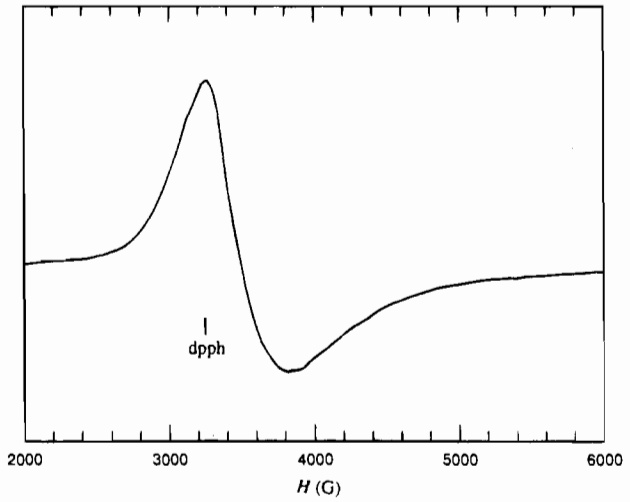

Figure 5. Powdered sample X-band EPR spectrum of compound **7** in the range 2000−6000 G. The intensity is arbitrary.

It follows that, as far as $|\delta| > h\nu$, $H_\perp$ increases with increasing $|D|$ whereas $H_\parallel$ should depend on the single-ion g factor only. Simulation of the EPR spectra of compound **17** showed that $|D| \approx |\delta|$, both parameters being much larger than the microwave quantum energy $h\nu$.[39]

For compound **7** a single, though anisotropic, line is observed at a g_{eff} value not far from that expected for the single-ion, which means that $|D| < |\delta|$. The shape of the observed signal can be reproduced assuming the linewidth to be markedly anisotropic, with $\Delta H_\perp > \Delta H_\parallel$. According to this simplified model, Heisenberg-exchange interactions provide the main contribution to the splitting of the ground state of the trimer, therefore supporting the perturbative approach which leads to (5). Significant departures from C_{3v} idealized symmetry are indeed observed in complex **7** and it is well-known that, in the limit of weak interactions, the value of J is very sensitive to small angular changes or distortions.[37]

Conclusions

The triiron(III) cluster $KFe_3(OCH_3)_7(dbm)_3 \cdot 4CH_3OH$ (**7**) has been synthesized by reaction of iron(III) chloride and H*dbm* in the presence of excess potassium methoxide. The arrangement of the oxygen atoms in the core of **7** reproduces a fragment of a *cp* lattice whose octahedral holes are occupied by the metal atoms. The structural similarities with bulk iron oxides and hydroxides such as α-Fe_2O_3, α-FeO(OH), and γ-FeO(OH) provide a clear example of the link between nanostructured molecular materials and extended systems. The magnetic behavior of **7** is consistent with the presence of antiferromagnetic exchange interactions between the metal centers. With respect to "basic" iron carboxylates, a much weaker metal-to-metal coupling is observed. This can be rationalized on the basis of the structural differences between **7** and μ_3-oxo-centered carboxylates. The splitting of the 4-fold ^2E electronic ground state of the cluster is attributed mainly to geometrical distortions from trigonal symmetry, which result in significant inequality of the exchange coupling interactions. Antisymmetric exchange contributions, detected by low-temperature EPR spectra, seem to play a minor role, a situation which contrasts with that encountered in $[Fe_3O(CH_3CO_2)_6(H_2O)_3]Cl \cdot 4H_2O$.

Our current research is aimed at tuning the experimental conditions so as to favor the growth of these iron(III)−alkoxide aggregates.

Acknowledgment. We gratefully acknowledge Prof. S. J. Lippard of MIT for a helpful discussion. This work was supported by the Human Capital and Mobility Program through Contract ERBCHRX-CT920080 and by "Ministero dell' Università e della Ricerca Scientifica e Tecnologica" (MURST) of Italy. We are grateful to the "Centro Interdipartimentale di Calcolo Automatico ed Informatica Applicata" (CICAIA) of Modena University for computer facilities.

Supporting Information Available: A full listing of crystal and experimental parameters and of bond distances and angles, anisotropic thermal parameters for non-hydrogen atoms, fractional coordinates and isotropic thermal parameters for hydrogen atoms, and selected O···O separations within oxygen layers (10 pages). Ordering information is given on any current masthead page.

IC950037Y